X-ray absorption near-edge structure of selenium in the Cu-In-Se system

2001 J. Phys.: Condens. Matter 13 4457

(http://iopscience.iop.org/0953-8984/13/20/307)

INSTITUTE OF PHYSICS PUBLISHING JOURNAL OF PHYSICS: CONDENSED MATTER

J. Phys.: Condens. Matter **13** (2001) 4457–4470 www.iop.org/Journals/cm PII: S0953-8984(01)22172-9

X-ray absorption near-edge structure of selenium in the Cu–In–Se system

A Wolska[1], R Bacewicz[1,3], J Filipowicz[1] and K Attenkofer[2]

[1] Faculty of Physics, Warsaw University of Technology, ul. Koszykowa 75, 00-662 Warsaw, Poland
[2] HASYLAB at DESY, Nottkestrasse 85, D-22603 Hamburg, Germany

E-mail: bacewicz@if.pw.edu.pl

Received 20 February 2001, in final form 10 April 2001

Abstract

The x-ray absorption near edge structure (XANES) of selenium is investigated in the crystals with compositions from the pseudobinary cut line Cu_2Se–In_2Se_3. This includes $CuInSe_2$, indium-rich ternary compounds ($Cu_2In_4Se_7$, $CuIn_3Se_5$, $CuIn_5Se_8$, $CuIn_7Se_{11}$) and α-In_2Se_3. The absorption at the K and L_3/L_2 edges of selenium has been measured using synchrotron radiation. Two theoretical approaches are used to the interpretation of the experimental data: the band structure calculation and the real-space multiple-scattering (RSMS) method. In the first one, the angular momentum projected densities of states at Se sites are calculated for $CuInSe_2$ and α-In_2Se_3 for the energies up to 17 eV above the conduction band minimum by the LMTO–ASA method. The RSMS approach represented by the FEFF8 code is used to calculate the XANES spectra for the phases with tetragonal symmetry. Clusters up to 160 atoms are used in the calculations. The influence of different structural factors on the selenium XANES is studied.

1. Introduction

Good perspectives for $CuInSe_2$ based solar cells (18% efficiency achieved) caused increased interest in other compounds from the Cu–In–Se system. Several phases have been identified in the Cu–In–Se ternary system along (or close to) the Cu_2Se–In_2Se_3 pseudobinary tie line [1, 2]. According to the phase diagram by Boehnke and Kuhn [1], only four ternary phases exist on the indium-rich side of the line: the α-phase of ordered $CuInSe_2$ (chalcopyrite structure) with homogeneity region from 47.5 to 55 mol% In_2Se_3, the β-phase (tetragonal, chalcopyrite-like defect structure) extending from 66.5 to 79.0 mol% In_2Se_3, the γ-phase (hexagonal or trigonal) 82 to 90 mol% In_2Se_3 and the δ-phase representing the homogeneity region of disordered $CuInSe_2$.

[3] Corresponding author.

A number of compounds belonging to the β-phase have been identified with various nominal compositions like $Cu_3In_5Se_9$, $Cu_2In_4Se_7$, $CuIn_3Se_5$ and $CuIn_5Se_8$ [1, 3]. The indium-rich phases attracted much attention when the existence of a thin layer of $CuIn_3Se_5$ on the surface of the absorber film in $CuInSe_2$-based solar cells was postulated [4]. Though it is still disputed whether such a film of a separate crystallographic phase really forms on the top of the $CuInSe_2$ film, the structural and electronic properties of the indium-rich phases are of basic and practical importance. Their structure is usually viewed as a $CuInSe_2$ chalcopyrite lattice with an incorporated ordered array of defects (copper vacancies or V_{Cu}–In_{Cu} defect pairs [5, 6]), so they are referred to as the ordered defect compounds (ODCs) or the ordered vacancy compounds (OVCs). Despite some evidence for the defect ordering stemming mostly from the electron diffraction [3, 7], present structural data do not provide enough evidence in favour of such ordering. According to Hanada *et al* [8], the $CuIn_3Se_5$ structure is built of three kinds of local Se tetrahedron and it is not an ordered vacancy compound.

In the composition range of the γ-phase, the structure is determined by the stacking of the close packed selenium layers. A number of polytype layered structures are formed with different sequences of a cubic and hexagonal stacking of the layers [2, 9, 10]

Apart from $CuInSe_2$, there are relatively scarce data on the electronic structure of ternary compounds belonging to these phases. The band structure calculations were performed for $CuIn_5Se_8$ with a hypothetical ordered defect structure [5, 11] and for $CuIn_3Se_5$ with the stannite structure [12]. Widening of the band gaps due to the weaker p–d repulsion than in $CuInSe_2$ is predicted. No data on the conduction band density of states have been published. The energy gaps for $Cu_2In_4Se_7$, $CuIn_3Se_5$ and $CuIn_5Se_8$ determined from the optical absorption are close to 1.3 eV [13].

X-ray absorption near edge structure (XANES) provides information on a local electronic structure at the site of an absorbing atom. It is sensitive to a local geometry and the bonding of atoms. If we neglect many-body effects, XANES reflects the local density of unoccupied states, provided the transition matrix element can be considered constant in the measurement range. Thus, it gives structure of the conduction band in semiconductors. Due to the dipole transitions selection rules, the XANES spectra taken at the K edge of an element probe the p-like electronic density of states around the absorbing atom. The L_3/L_2-edge XANES gives information about the d-like (and to lesser extent s-like) local density of states.

In [14] we published results on the XANES spectra of $CuInSe_2$ crystals measured at the K edges of Cu and Se, the L_1 edge of In and the L_3 edges of all three elements. The present study deals with the XANES investigation of a number of phases from the pseudobinary tie line $(Cu_2Se)_x(In_2Se_3)_{1-x}$ for x values from 0 (In_2Se_3) to 0.5 ($CuInSe_2$). A short account of these results has been given in [15]. On the copper-rich side, the end of the line compound Cu_2Se has been included in our study. This paper is concentrated on the selenium K and L_3 edge absorption spectra and their evolution along the pseudobinary line, since the most significant changes in the local environment can be expected for selenium atoms.

2. Calculations

The interpretation of the experimental data is based either on the band structure calculations by the linear muffin tin orbital (LMTO) method or alternatively on the real-space multiple-scattering (RSMS) approach represented by the FEFF8 code [16]. The first method is suitable in the case of a well defined long range symmetry. The RSMS method uses atomic clusters and is convenient in the case of defected or disordered structures. It also includes the core-hole effects that are not taken into account in the LMTO calculation.

The LMTO method in the atomic sphere approximation [17] has been used for the calculation of the angular momentum projected local density of states (LDOS) for $CuInSe_2$ and In_2Se_3 compounds. A muffin-tin potential has been generated self-consistently for the unit cell containing 16 muffin-tin non-equivalent spheres (two Cu, two In, four Se and eight empty spheres) for $CuInSe_2$ and 13 (three Se, two In and eight empty spheres) for In_2Se_3. The 'l' expansion is truncated to $l = 2$ in the copper, selenium and empty spheres and to $l = 3$ in the indium spheres. This gives satisfactory convergence for the energies below 1 Ryd, i.e. in the energy range where we use the band structure approach for the XANES interpretation. Other details of calculations are the same as in [14]. The local angular momentum projected densities of states have been calculated as a final step in the LMTO calculation. In order to compare the results of the calculation to the XANES spectra, the raw LDOS curves have been broadened by the convolution with a Lorentzian profile. We took the broadening parameter 2.2 eV for the p-like LDOS and 2 eV for the s- and the d-like LDOS. These values represent the total broadening of the K- and L_3-edge spectra estimated from the fit of the arctan function to the edge jump (see also section 4.2 in this paper). Figure 1 presents the selenium LDOS curves for the different state symmetries. The limitation of the calculated LDOS data in the interpretation of the x-ray absorption is the failure to describe the absorption plateau above 12 eV corresponding to the 'quasi-continuum' of states. This is due to the limited basis set used in the calculation.

In the RSMS approach, a cluster of atoms surrounding an absorbing atom represents the real structure of the solid. The *ab initio* calculations with the local potential described in the muffin-tin approximation are performed self-consistently [16]. Coordinates of the atoms in the cluster were given as the input data. The Hedin–Lundquist exchange–correlation potential was used. The presence of a fully relaxed core hole was taken into account. The full multiple scattering calculations (up to infinite order) were performed for clusters containing 32 atoms. The clusters up to 160 atoms have been used to calculate XANES. The RSMS method quite often fails to describe properly the threshold region of the spectra. Reasons for that are the limited cluster size and drawbacks of the muffin-tin approximation close to the muffin-tin zero.

3. Experiment

3.1. Crystals

The crystals used in this study were grown by the vertical gradient freezing method. The starting melts had compositions within the 50–85 mol% In_2Se_3 range. After equilibration at 1050 °C, the melt was cooled to 750 °C with the cooling rate of 1 °C/hour. In most cases we obtained large grain polycrystalline material. The ingots exhibited a strong segregation effect with the indium content increasing along the growth direction. Crystal composition was determined by the electron microprobe. Deviation of the composition from the pseudobinary tie line Cu_2Se–In_2Se_3 did not exceed the accuracy of the microprobe measurements, so we dealt essentially with the phases from the pseudobinary cut.

The indium-rich side of the ingot (last to grow) was a layered, easily cleaved and soft crystal in contrast to the hard main part of the ingot. It corresponds to the Boehnke γ-phase [1]. The x-ray Laue pattern of the crystals showed the hexagonal ordering with the c-axis perpendicular to the cleavage plane. The most common composition of crystals for this part of the bulk corresponds to 86 mol% In_2Se_3, which is equivalent to a nominal $CuIn_6Se_{9.5}$ formula (it corresponds to the ε-phase of Folmer *et al* [2]). We also separated flakes with the composition $CuIn_7Se_{11}$.

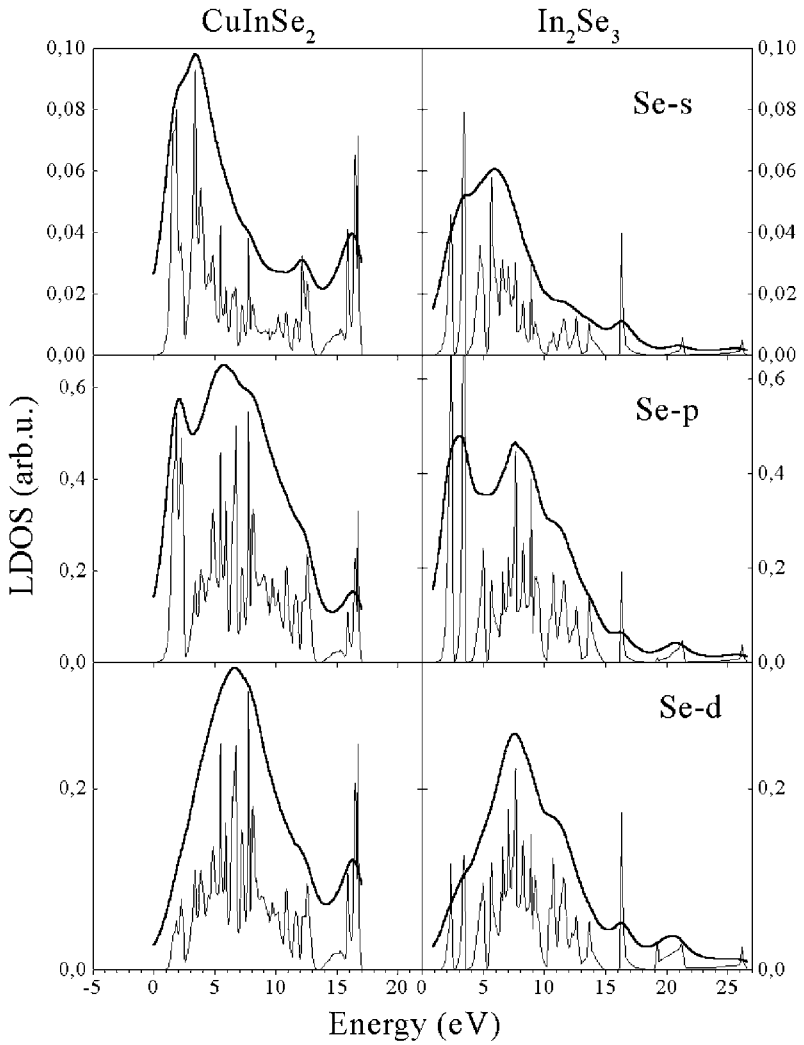

Figure 1. Conduction band density of states at a Se site in $CuInSe_2$ and In_2Se_3 (raw data—thin curve, broadened LDOS—thick curve). The zero energy coincides with the bottom of the conduction band.

The samples from the border between the soft, layered part of the crystal and the hard one had a typical composition Cu 7.0–7.5 at.%, In 35–37 at.%, Se 55–57 at.%. It is close to the nominal formula $CuIn_5Se_8$. We found crystals with this composition having tetragonal as well as hexagonal symmetry. It is in keeping with the results of Frangis *et al* [10] and Manolikas *et al* [9], who identified $CuIn_5Se_8$ phases of both symmetries. Recently, tetragonal and hexagonal thin films of $CuIn_5Se_8$ have been prepared by Kohara *et al* [18].

Samples of other tetragonal phases with nominal compositions $Cu_3In_5Se_9$, $Cu_2In_4Se_7$ and $CuIn_3Se_5$ were cut out from the main part of the ingot. Homogeneity of the samples across the bulk was approximately 0.5 at.%.

Apart from the ternary phases, we grew crystals of the binary compounds from the both ends of the pseudobinary line: Cu_2Se and In_2Se_3. The structure of In_2Se_3 crystals has been

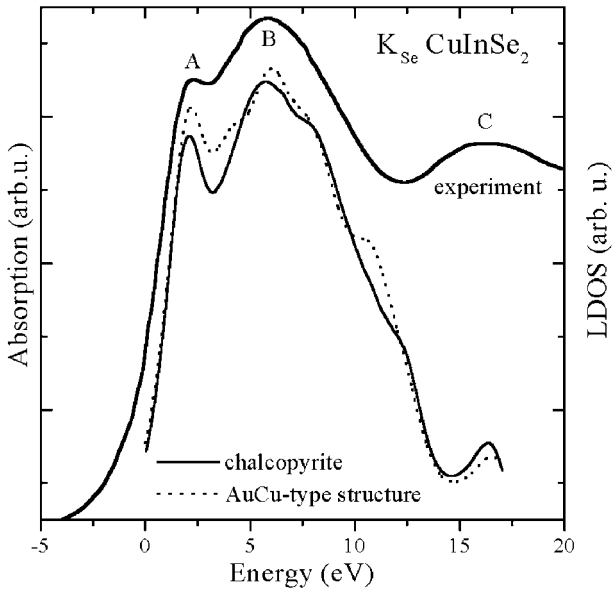

Figure 2. Selenium K-edge absorption in $CuInSe_2$ compared to the p-like LDOS for two structures: chalcopyrite and AuCu-type structure.

determined to be the rhombohedral α-phase with the space group $R3m$ [19]. The crystallized Cu_2Se bulk appeared to be multiphase material and we used it only for reference purposes.

For all measurements we used cleaved samples of the layered phases and polished ones of the tetragonal phases.

3.2. Measurements

The K-edge absorption was measured at HASYLAB, Hamburg. The measurements were carried out in the transmission mode at the A1 station (HASYLAB). The high-resolution four-crystal mode was used. The resolution was about 0.5 eV at 10 keV. The samples were prepared either by dusting a fine ground powder onto Scotch tape or by making cellulose based pills with appropriate amount of the powder. The measurements were performed on samples with different thickness to eliminate the 'thickness effect' [20]. The XANES spectra in the soft x-ray range (L_3/L_2 edge of Se) were measured at the SUPERACO ring at LURE, Orsay (SU22 station) in the total yield mode. Special attention was paid to a proper surface preparation of the crystals. No anisotropy of the XANES was studied.

4. Results and discussion

4.1. K-edge absorption

4.1.1. $CuInSe_2$. $CuInSe_2$ near-edge absorption structure has been discussed in the previous paper [14]. Here we present some results of the calculations by the LMTO method and the RSMS method. Their aim is to assess the sensitivity of the XANES spectra to various structural factors of $CuInSe_2$.

One of them is the coexistence of chalcopyrite and CuAu-like structures in $CuInSe_2$ anticipated by Wei *et al* [21]. Figure 2 presents the absorption plot compared with the LMTO

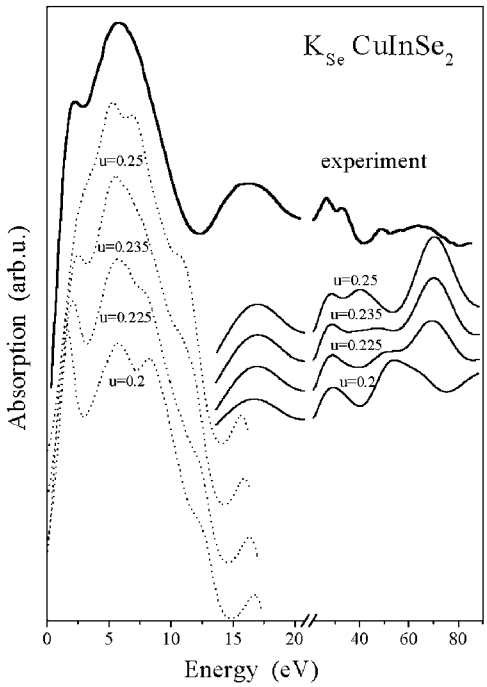

Figure 3. Comparison of the K-edge absorption with the LDOS (dotted curve) and FEFF8 calculated XANES (thin solid curve) for different u values.

calculated Se p-like density of states for these two structures. The origin of the energy scale is at zero energy of the LDOS plot and coincides with the Fermi energy. We can see that the expected differences in the electronic structure of the conduction band are quite small, and the XANES data cannot discriminate between two structures. Also the FEFF8 calculation does not show any differences.

An important structural parameter in the chalcopyrite structure is the position of the selenium atom in the unit cell. A deviation of this, the so called anion parameter u, from 0.25 reflects the deviation from the ideal tetrahedral position and is a manifestation of differences in the R_{Cu-Se} and R_{In-Se} bond lengths. The u value strongly influences electronic properties of the compounds [22, 23]. Figure 3 shows the p-like LDOS calculated for different u values and the XANES curves calculated by the FEFF8 code for the energies above 13 eV. These results confirm the dependence of the conduction band structure on the u value. The best overall match to the experimental data is seen for the $u = 0.225$ value. It agrees with the Rietveld refined x-ray diffraction data $u = 0.2252$ [24].

4.1.2. In_2Se_3. The $x = 0$ boundary of the pseudobinary $(Cu_2Se)_x(In_2Se_3)_{1-x}$ cut line is the In_2Se_3 compound. A number of crystallographic phases has been reported for In_2Se_3 [25, 26]. According to the x-ray diffraction and the Raman study [19], the crystals used in this investigation belong to the layered α-phase with the rhombohedral symmetry, space group $R3m$. The basic layer set consists of five layers, Se–In–Se–In–Se. According to our x-ray diffraction data, half of the In atoms have octahedral bonds and half tetrahedral ones. This is in keeping with the structural model given in [25] and contradicts the findings of [26], where only tetrahedrally coordinated indium is assumed. Selenium atoms in α-In_2Se_3 have predominantly tetrahedral coordination; however some of them are one and three coordinated.

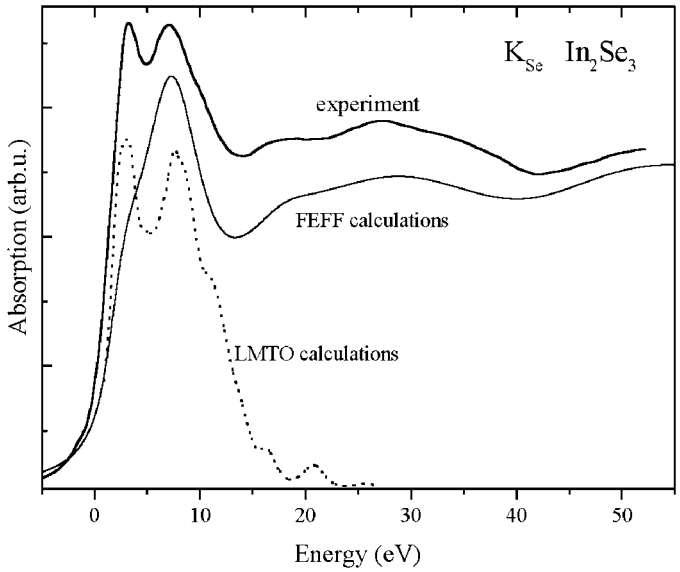

Figure 4. K-edge absorption in In_2Se_3 compared with the p-like LDOS (dotted curve) and FEFF8 calculated plot (thin solid curve).

This makes the main difference comparing to $CuInSe_2$, which has only fourfold coordinated selenium. Figure 4 presents the x-ray absorption at the selenium K edge of α-In_2Se_3 in the relative energy scale. The experimental results are compared to the broadened LMTO p-like LDOS for the 0–17 eV energy range and to the theoretical curve calculated within the RSMS approach for the energies up to 50 eV. The XANES is properly though qualitatively reproduced within such a combined approach.

4.1.3. In-rich ternary phases. Figure 5 shows the evolution of the selenium K-edge XANES along the Cu_2Se–In_2Se_3 pseudobinary tie line. Two crystal phases of $CuIn_5Se_8$ have been investigated: tetragonal (T) and hexagonal (H). The largest changes are visible in the structure of the first strong maximum of the spectra, the so called, white line. For $CuInSe_2$, this structure was assigned to the features of the p-type LDOS. According to the LMTO calculations [14], the first peak (A) at 2.2 eV (in the relative energy scale—figure 2) corresponds to the In(s, p)–Se(p) antibonding orbital. Its bonding counterpart is located 6 eV below the valence band maximum [20]. The maximum at 6.5 eV (B) reflects, in the case of $CuInSe_2$, the strongest feature in the Se p-like density of states hybridized with Cu(s) and In(p) states.

The A peak is connected to the indium presence and practically disappears for Cu_2Se. Its intensity increases for growing In concentration. This reflects an increasing contribution of indium to the bonding in these materials. The B feature has the same shape and comparable intensity for the end compositions and for $CuInSe_2$, but has much lower intensity for the defected tetragonal phases from $Cu_2In_4Se_7$ (67 mol% In_2Se_3) to tetragonal $CuIn_5Se_8$ (83 mol% In_2Se_3). For the hexagonal $CuIn_5Se_8$ and the phases with a higher content of indium the B feature has the intensity close to that of In_2Se_3.

The structures studied here are based on the tetrahedrally coordinated selenium. However, in the α-In_2Se_3 layered phase one-, three- and four-coordinated selenium atoms are present. We can expect such a multicoordination of Se atoms also for the layered ternary phases with a high content of indium. This can explain the qualitative change in the spectra at the In_2Se_3

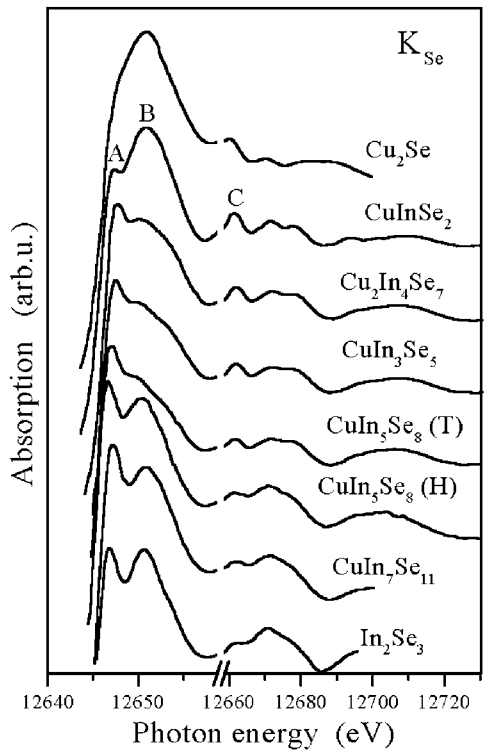

Figure 5. Evolution of the K-edge absorption for the Cu–In–Se system. The upper part of the absorption curves has been blown up to show details.

Table 1. The lattice constants and the bond lengths of tetragonal Cu–In–Se phases.

Compound	a (Å)	c (Å)	R_{Cu-Se} (Å)	R_{In-Se} (Å)
$CuInSe_2$	5.7837	11.6234	2.428	2.594
$CuIn_3Se_5$	5.76	11.53	2.449	2.618
$CuIn_5Se_8$ (T)	5.751	11.523	2.479	2.621

concentration corresponding to the $CuIn_5Se_8$ composition, for which two phases, tetragonal and layered hexagonal, coexist [9, 10]. It is seen that tetragonal $CuIn_5Se_8$ has XANES very similar to other In-rich tetragonal phases (e.g. $CuIn_3Se_5$), whereas hexagonal $CuIn_5Se_8$ exhibits a spectrum similar to In_2Se_3.

The structure of tetragonal Cu–In–Se phases can be built of three types of tetrahedron representing different local environments of Se. Based on the condition of the minimal deviation from the electron octet rule, three types of tetrahedron were proposed [6] with eight, seven and nine valence electrons respectively:

(A) 2Cu + 2In
(B) V_{Cu} + Cu + 2In
(C) V_{Cu} + 3In.

Discussing structural data for $CuIn_3Se_5$ Hanada *et al* [8] included also a local tetrahedron with ten valence electrons:

(D) Cu + 3In.

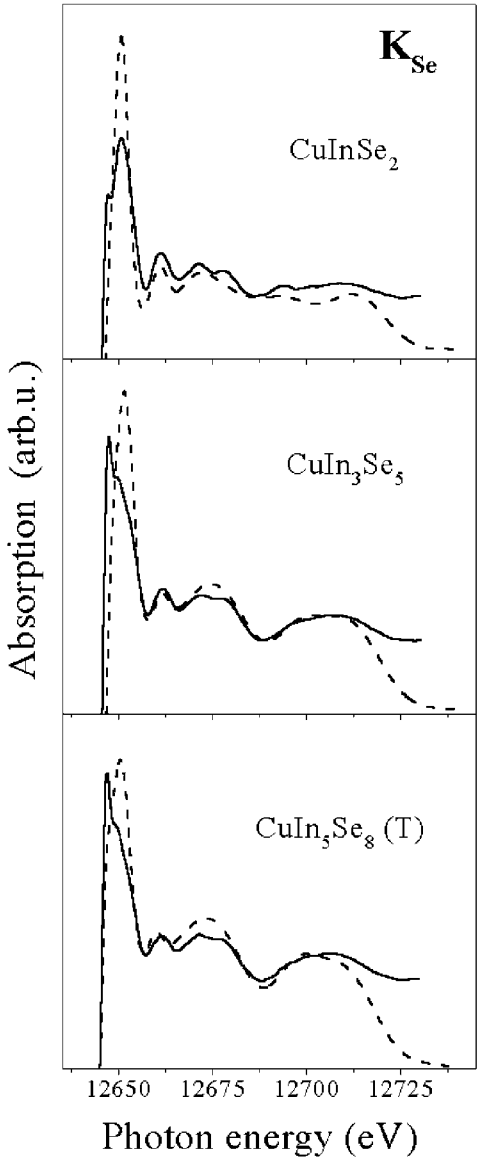

Figure 6. Comparison of the Se K-edge absorption (solid curve) with results of FEFF8 calculations (dashed curve) for three tetragonal phases.

We used, however only tetrahedra (A)–(C) for modelling the structure.

The structure of $CuInSe_2$ contains only A-type tetrahedra, whereas the structure of $CuIn_3Se_5$ can be built of 20% A tetrahedra and 40% B and C tetrahedra each, or alternatively 60% B, and 20% C and 20% D. Tetragonal $CuIn_5Se_8$ is built from 50% B and 50% C tetrahedra.

The most efficient way of modelling the structure of the In-rich compounds consists in incorporating an ordered array of the defect pairs ($2V_{Cu} + In_{Cu}$) into $CuInSe_2$. We did it for $CuIn_3Se_5$ and tetragonal $CuIn_5Se_8$ taking into account the average bond lengths for these two compounds determined from the EXAFS data (table 1). As a result, the unit cells have been

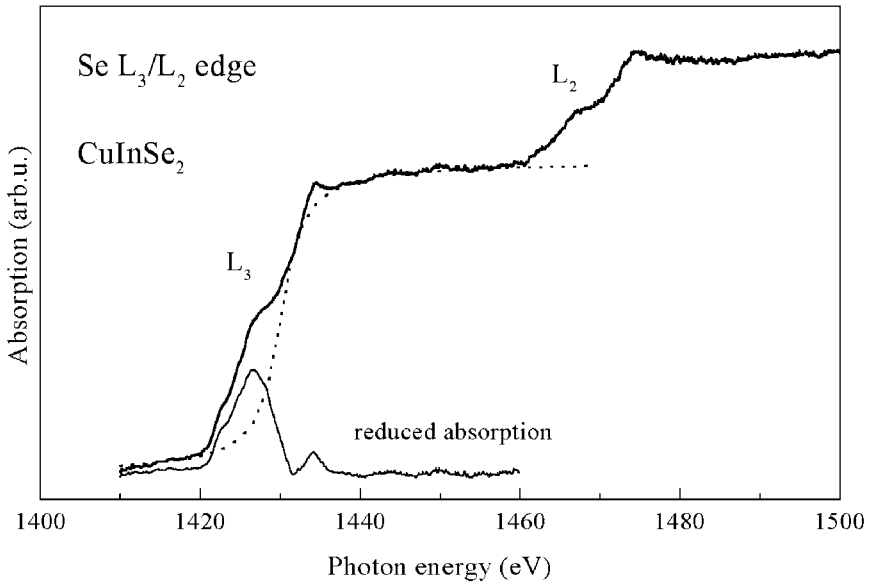

Figure 7. Selenium L_3/L_2-edge absorption for $CuInSe_2$. The dotted curve represents an arctangent function; the thin solid curve is a difference plot (reduced absorption).

defined for both structures. For $CuIn_3Se_5$ its size in the *c*-axis direction is five times the *c*-axis of the respective chalcopyrite cell. The space group of this structure is $I\bar{4}$. $CuIn_5Se_8$ structure has the unit cell with the size of chalcopyrite cell and $P\bar{4}$ space group. Using these structures, clusters of up to 160 atoms (radius 10 Å) have been created for the RSMS calculations.

Figure 6 shows the results of the FEFF8 calculations for three tetragonal phases compared to the experimental data. Due to the well known limitations of the RSMS method, theoretical plots do not reproduce the first maximum of the XANES. The higher energy part (up to 80 eV above the edge) of the XANES is reproduced by the RSMS method with a comparable matching quality for all three structures. This indicates that the structures of $CuIn_3Se_5$ and tetragonal $CuIn_5Se_8$ were chosen properly. It has to be stressed, however, that the result of the presented calculations does not depend on the defect ordering.

4.2. Selenium L_3/L_2 edges

Selenium L_3/L_2 edge absorption is due to transitions from $2p_{3/2}$ ($2p_{1/2}$) core states to s- and d-like unoccupied states. As has been proved for $CuInSe_2$ by the calculation of the relative oscillator strengths for the transitions to s and d symmetry states of selenium [14], the XANES spectra at the L_2/L_3 edges of selenium is dominated by the d-like LDOS. The intensity ratio of the L_3 to L_2 absorption step should be 2 due to the degeneracy of the final states. Other differences between L_2 and L_3 edges arise from the Coulomb and spin–orbit interactions in the final state. Since these effects are expected to be small for Se^{2-} ions and because the L_2 absorption appears on the background from the transitions from the L_3 edge, in the further analysis we limit ourselves to the L_3 absorption.

Figure 7 presents the XANES for $CuInSe_2$. It shows a steplike behaviour with some structure in the edge region. In order to elucidate this structure, the broadened step absorption representing transitions to a quasi-continuum of states was subtracted from the absorption

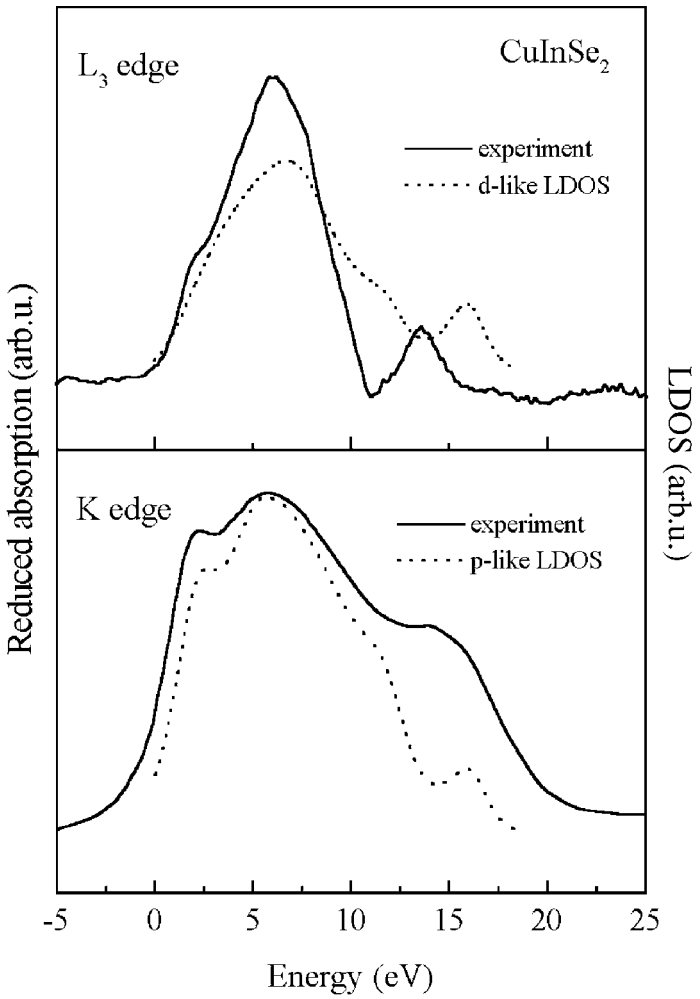

Figure 8. Comparison of the reduced absorption for the L_3 and K edges of $CuInSe_2$ with the LDOS.

curve. The step absorption convoluted with a Lorentzian with a half-width Γ is described as

$$\mu = \mu_0 \left[\frac{\pi}{2} + \arctan\left(\frac{2(\hbar\omega - E_0)}{\Gamma} \right) \right].$$

Figure 8 shows comparison of the reduced absorption with the d-like LDOS curve. For comparison, the reduced K-edge spectrum of $CuInSe_2$ is shown together with the corresponding p-like LDOS. The first two features at the L_3 XANES match the structure at the K-edge spectra. The shoulder at 2.5 eV corresponds to d-like states at the bottom of the conduction band hybridized with the low-lying p-like states responsible for the analogous structure in the K-edge XANES (A). The main maximum of the reduced spectrum at 6.5 eV corresponds to the main broadened band of the Se d-like LDOS. The peak at 14 eV corresponds to the peak at 16 eV seen in the K-edge absorption both for Se and Cu [14]. The K-edge peak position agrees with the position of the respective peak in the LMTO calculated LDOS. It is due to Cu(p) and In(p) states hybridized with the Se d states. It is difficult at the moment to explain

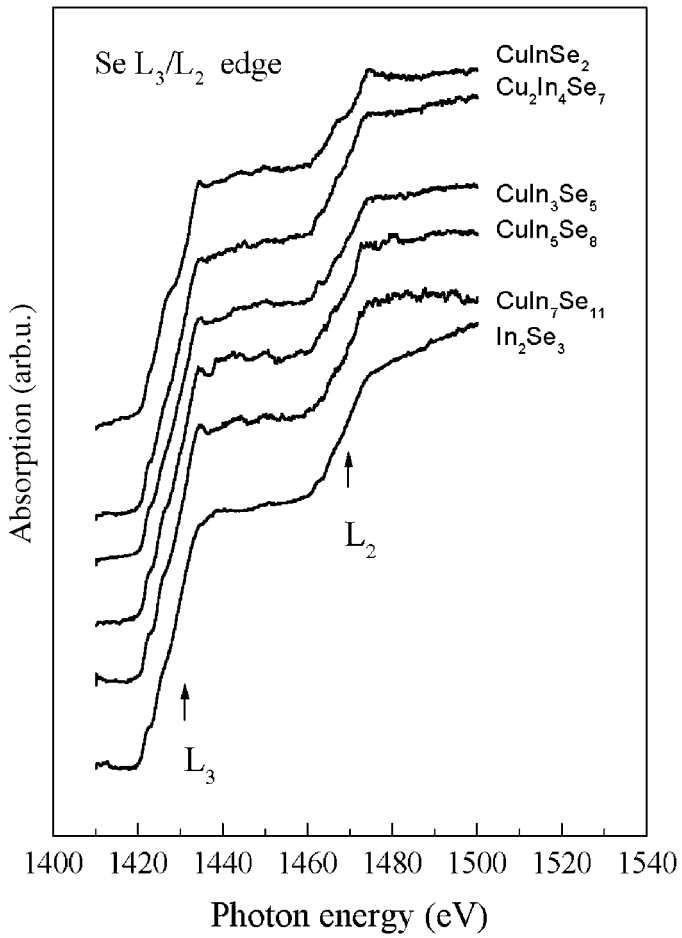

Figure 9. Selenium L_3/L_2 absorption for the In-rich compounds.

the energy shift between the 14 eV peak at the L_3 spectrum and the feature seen at 16 eV in the Se d-like LDOS. The most likely reason is the core-hole effect not taken into account in the LMTO calculations. Many body effects are known to change the energy scale in the case of L_3 edges significantly when comparing with the ground state LDOS [27].

Figure 9 presents absorption curves for a number of the In-rich phases. The intensity ratio between the L_3 and L_2 absorption step is for most of the phases 10–20% larger than the statistical value 2. The curves of the reduced L_3 absorption are shown in figure 10. In the reduction process the same parameters $E_0 = 1430$ eV and $\Gamma = 4$ eV were used for all phases. The curve for $CuInSe_2$ differs from the others, which are of comparable intensity but broadened. When we compared intensities of the shoulder at 2.5 eV taken in respect to the main peak we found that it exhibits the same evolution with a changing In concentration as the analogous structure (A) in the K edge spectra. This indicates that it is due to Se d states hybridized with Se p states contributing to the antibonding In(s)–Se(p) orbital. The peak at 14 eV has comparable intensity in all ternary phases and practically disappears in the In_2Se_3 plot. This confirms strong admixture of Cu states in the respective LDOS feature.

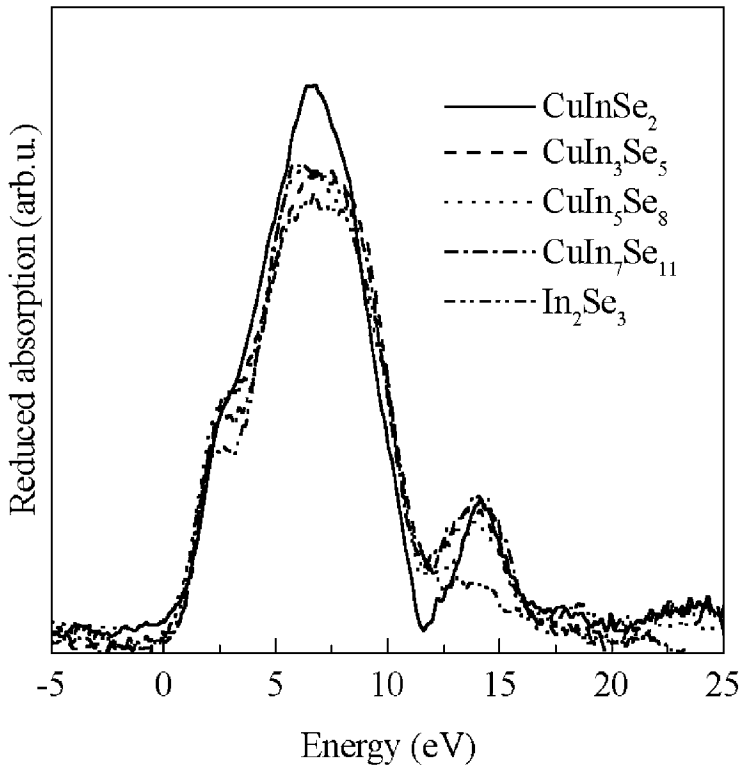

Figure 10. Comparison of the L_3 reduced absorption for a number of Cu–In–Se compounds.

5. Conclusions

XANES of selenium at the K and L_3/L_2 edges has been studied for the crystals of the compounds along the Cu_2Se–In_2Se_3 pseudobinary line. Relatively small changes are observed in both the K-edge and L_3-edge XANES in agreement with the calculations of Zhang *et al* [6], who found that a change of the bonding charge surrounding the Se atom is small in these phases. The main differences are seen in the low energy part of the K-edge spectra. They have been interpreted on the basis of the LMTO calculations performed for $CuInSe_2$ and In_2Se_3. Differences in the spectra of the tetragonal and layered hexagonal $CuIn_5Se_8$ compound reflect the change in the coordination of selenium in these two structures. The XANES of the layered Cu–In–Se phases with a composition close to In_2Se_3 resembles that of the binary compound. The K-edge XANES was calculated by the real-space multiple-scattering method for the modelled structures of two tetragonal phases $CuIn_3Se_5$ and $CuIn_5Se_8$. The obtained match to the experimental data is of comparable quality as for $CuInSe_2$. Though we used an ordered distribution of copper vacancies in these structures rather than a statistical one, the selenium XANES seems not to depend significantly on the ordering.

In the case of $CuInSe_2$, both the band structure calculation and the RSMS approach show the sensitivity of the XANES to a value of the anion displacement parameter. This reflects the already established importance of the u value in determining the electronic structure of chalcopyrite semiconductors. The XANES, however, is insensitive to possible polytype variations of the $CuInSe_2$.

Acknowledgments

Support was provided by the Polish State Committee of Scientific Research under grant 05/T11/98/6A. We acknowledge the assistance of Dr Philippe Sainctavit from LURE (Orsay).

The TB–LMTO–ASA calculations have been performed with the code developed by O K Andersen and O Jepsen and kindly provided by them.

References

[1] Boehnke U-C and Kuhn G 1987 *J. Mater. Sci.* **22** 1635
[2] Folmer J C W, Turner J A, Noufi R and Cahen D 1985 *J. Electrochem. Soc.* **132** 1319
[3] Tseng B H and Wert C A 1989 *J. Appl. Phys.* **65** 2254
[4] Schmid D, Kessler J and Schock H W 1994 *Proc. 12th Eur. Photovoltaic Solar Energy Conf. (Amsterdam)* p 653
[5] Wei Su-Huai 1997 *Proc. 11th Int. Conf. on Ternary and Multinary Compounds (Salford) (Inst. Phys. Conf. Ser. 152)* (Bristol: Institute of Physics) p 765
[6] Zhang S B, Wei Su-Huai and Zunger A 1998 *Phys. Rev.* B **57** 9642
[7] Xiao H Z, Chung Yang L and Rockett A 1994 *J. Appl. Phys.* **76** 1503
[8] Hanada T, Yamana A. Nakamura Y, Nittono O and Wada T 1997 *Japan. J. Appl. Phys.* **36** L1494
[9] Manolikas C, Van Landuyt J, De Ridderand R and Amelinckx S 1979 *Phys. Status Solidi* a **55** 709
[10] Frangis N, Van Tendoloo G, Manolikas C, Van Landyut J and Amelinckx S 1986 *Phys. Status Solidi* a **96** 53
[11] Wei Su-Huai and Zunger A 1996 *Cryst. Res. Technol.* **31** 81
[12] Suzuki M, Uenoyama T, Wada T, Hanada T and Nakamura Y 1997 *Japan. J. Appl. Phys.* **36** L1139
[13] Bacewicz R, Filipowicz J and Wolska A 1997 *Proc. 11th Int. Conf. on Ternary and Multinary Compounds (Salford) (Inst. Phys. Conf. Ser. 152)* p 507
[14] Bacewicz R, Wolska A, Lawniczak-Jablonska K and Sainctavit P 2000 *J. Phys.: Condens. Matter* **12** 7371
[15] Bacewicz R, Wolska A, Filipowicz J and Lawniczak-Jablonska K 2000 *Proc. 12th Int. Conf. on Ternary and Multinary Compounds (Hsinchu) Japan. J. Appl. Phys.* at press
[16] Ankundinov A L, Ravel B, Rehr J J and Conradson S D 1998 *Phys. Rev.* B **58** 756
[17] Andersen O K 1975 *Phys. Rev.* B **12** 3060
[18] Kohara N, Nishiawaki S, Negami T and Wada T 2000 *Japan. J. Appl. Phys.* **39** 6316
[19] Lewandowska R, Bacewicz R and Filipowicz J 2001 *Mater. Res. Bull.* at press
[20] Heald S M and Stern E A 1977 *Phys. Rev.* **12** 5549
[21] Wei Su-Huai, Mattila T, Zhang S B and Zunger A 2000 *12th Int. Conf. on Ternary and Multinary Compounds (Hsinchu) Japan. J. Appl. Phys.* at press
[22] Jaffe J E and Zunger A 1983 *Phys. Rev.* B **28** 5822
[23] Jaffe J E and Zunger A 1984 *Phys. Rev.* B **29** 1882
[24] Paszkowicz W, Lewandowska R and Bacewicz R 2000 *Rietveld Conf. (Wisla)*
[25] Ye J, Soeda S, Nakamura Y and Nittono O 1998 *Japan. J. Appl. Phys.* **37** 4264
[26] Ishikawa M and Nakayama T 1998 *Japan. J. Appl. Phys.* **37** L1122
[27] Grunes L A 1983 *Phys. Rev.* B **27** 2111